

Crystalline Magnetic Order in a Dipolar Quantum Fluid

M. Vengalattore^{1,*}, J. Guzman¹, S. R. Leslie¹, F. Serwane¹, and D. M. Stamper-Kurn^{1,2}

¹*Department of Physics, University of California, Berkeley CA 94720*

²*Materials Sciences Division, Lawrence Berkeley National Laboratory, Berkeley, CA 94720*

(Dated: January 21, 2009)

We report on the magnetic phases of quasi-two dimensional ^{87}Rb $F = 1$ spinor gases produced by cooling unmagnetized gases into the regime of quantum degeneracy. We find a robust low temperature magnetic phase characterized by crystalline ordering of spin domains, an instance of spontaneously broken translational symmetry in a quantum fluid. This phase displays an emergent order parameter, a spin axis along which the magnetization shows the largest variance.

Coherent quantum fluids exhibiting spontaneous spatial order have garnered widespread attention in connection to possible supersolid phases of matter [1] and the ground states of high- T_c superconductors [2, 3] and other correlated electronic materials [4]. Such intrinsically heterogeneous quantum fluids may arise due to the interplay between multiple order parameters [4], the influence of adjacent ground states with differing tendencies [5] or the presence of competing interactions [6, 7].

Recent observations [8] hint at similar phenomenology in a magnetic quantum gas, the $F = 1$ spinor Bose gas of ^{87}Rb . Early studies of ^{87}Rb spinor condensates [9, 10] seemed to indicate that their magnetic properties were governed solely by their weak spin-dependent contact interaction. This interaction, with mean-field energy $-|c_2|n\langle\mathbf{F}\rangle^2$, favors spin states with maximum magnetization [11, 12]; here, c_2 is related to s -wave scattering lengths for interatomic collisions, n is the number density, and \mathbf{F} is the dimensionless vector spin. However, recent works [8, 13–15] point to the significance of magnetic dipolar interactions in determining magnetization dynamics and ordering in ^{87}Rb gases with large spatial extent. How the competition between the spatially isotropic contact interaction and the anisotropic long-range dipole interaction resolves itself at equilibrium remains an important open question.

Here, we address this question by examining the magnetic order in gases produced by cooling unmagnetized thermal spin mixtures into the regime of quantum degeneracy. At their lowest temperatures, these quantum fluids spontaneously break translational symmetry to arrive at a crystalline magnetic phase. We argue that this crystalline phase represents an unforeseen equilibrium texture of this dipolar fluid.

For our experiments, we prepared non-degenerate gases of ^{87}Rb with up to 4×10^7 atoms confined optically at the elliptical focus of a linearly polarized, 825 nm wavelength laser beam. These gases were characterized by fractional populations $(\zeta_1, \zeta_0, \zeta_{-1})$ in the three eigenstates of F_z , and were unmagnetized given the dual

constraints of $\zeta_1 = \zeta_{-1}$ (zero longitudinal magnetization) and negligible coherence among the sublevels (zero transverse magnetization). If $\eta = \zeta_0 - \zeta_1 \neq 0$, such mixtures do possess a non-zero magnetic quadrupole moment that explicitly breaks rotational symmetry. We focus on two particular cases. An $\eta = 1/4$ spin mixture was prepared by applying a resonant $\pi/2$ rf pulse to a longitudinally magnetized gas, and allowing for 75 ms of diffusive admixing in a 50 mG/cm magnetic field gradient to eliminate transverse coherence [16]. An $\eta = 0$ admixture was prepared by repeating this pulse/diffusion sequence several times.

Following their preparation, the spin mixtures were evaporatively cooled by gradually lowering the optical trap depth U . During this process, the trap frequencies, with initial values of $(\omega_x, \omega_y, \omega_z) = 2\pi(80, 800, 8) \text{ s}^{-1}$ at $U/k_B \simeq 9 \mu\text{K}$, decreased as $\omega_{x,y,z} \propto \sqrt{U}$ and the gas temperature was found to scale as $k_B T = 0.118(6)U$, with all Zeeman sublevels attaining the same temperature [17]. After the trap depth was reduced to the desired level, the spinor gas was allowed to equilibrate for up to 1 s.

The gas was then probed by either of two methods. The instantaneous column-integrated vector magnetization $\mathbf{M} = \mu\tilde{n}\mathbf{F}$ was measured in the \hat{x} - \hat{z} plane by magnetization-sensitive phase contrast imaging [16, 18]. Here, μ is the atomic magnetic moment and \tilde{n} is the local density of the gas integrated along the imaging axis (\hat{y}). Alternately, the atom number, temperature and condensate fraction for each Zeeman sublevel were measured by time-of-flight imaging techniques.

Throughout the evaporation and equilibration, a $B = 150$ mG magnetic field, varying by less than $5 \mu\text{G}$ across the extent of the gas, was applied along \hat{z} . This field produces a quadratic Zeeman shift of the form qF_z^2 with $q/h = (70 \text{ Hz/G}^2)B^2 = 1.5 \text{ Hz}$ that was much smaller than the strength of the contact and dipole interactions for the degenerate gases studied. The field also induces rapid (110 kHz) Larmor precession of the atomic spins, owing to which the magnetic dipole interactions assume a precession-averaged form [8, 15, 19].

We first consider spinor gases produced initially with $\eta = 0$. This mixture corresponds to the equilibrium state far from quantum degeneracy for our system where $k_B T \gg \{q, |c_2|n\}$. The bulk features of gases produced by cooling this initial mixture display several hallmarks

*Present address: Laboratory of Atomic and Solid State Physics, Cornell University, Ithaca, NY 14853.

Electronic address: mukundv@ccmr.cornell.edu

of Bose condensation. Gases probed after a time of flight show bimodal density distributions below T_{c,N_0} , the ideal-gas Bose-condensation temperature given the population N_0 of the $m_F = 0$ sublevel. The measured populations within the central peak and the gaussian wings, associated typically with the condensate and thermal fractions, respectively, match closely with those expected for scalar Bose gases.

However, *in situ* probing of these gases (Fig. 1) reveals the formation of unforeseen magnetic phases. Immediately below T_c , the spinor gas becomes spontaneously magnetized, explicitly breaking spin-rotational symmetry within a central region consistent with the spatial dimension of a Bose condensate. Further, this magnetization is inhomogeneous and forms a self-organized lattice of spin domains, explicitly breaking translational symmetry. The crystalline organization of these spin domains is demonstrated also in the spatial Fourier spectrum of the vector magnetization, $|\tilde{\mathbf{M}}(k_x, k_z)|^2$, by the peaks at wavevectors $k \simeq \pi/l$ where $l \sim 5 \mu\text{m}$ is the characteristic length scale of the domains (Fig. 2(b)). We observe that a rotation of the optical trap about \hat{y} causes a corresponding rotation in the orientation of the crystal, i.e. the orientation of the crystal in the \hat{x} - \hat{z} plane seems to be pinned to the boundaries imposed by the trap.

Spin textures with slightly different features were observed upon cooling unmagnetized thermal gases that possessed a non-zero quadrupole moment. While such mixtures do not represent the equilibrium distribution far from quantum degeneracy, the small cross-section for spin-mixing collisions prevented their equilibration to $\eta = 0$ within experimentally accessible timescales (seconds). However, below T_{c,N_0} , the thermal fraction of degenerate gases did reach equal populations in the three Zeeman sublevels, presumably due to the strong enhancement of spin-mixing collisions by the high density and bosonic enhancement intrinsic to a condensate [17].

Yet, in spite of this condensate-mediated spin mixing, the effects of the initial non-zero η were still visible in the magnetization textures of the degenerate gas. In contrast to the case of $\eta = 0$, for initial $\eta = 1/4$ we observe two distinct magnetic phases. Just below T_{c,N_0} , spin textures form that are fairly uniform with gradual modulations on the length scale of $100 \mu\text{m}$. Only at a distinctly lower temperature does the gas display the periodic spin modulations and spectral signatures of crystalline order. The cases of $\eta = 0$ and $\eta > 0$ also differ in the overall distribution of magnetization orientations. For $\eta = 0$, the magnetization orientation shows no preferred axis or plane, while for $\eta > 0$ the magnetization was found to lie predominantly in the \hat{x} - \hat{y} plane.

To characterize these magnetic orders, we quantified order parameters for the long-wavelength ferromagnetic order and the short-wavelength crystalline order. For this, spatial Fourier space was demarcated into regions shown in Fig. 2 and the integral of $|\tilde{\mathbf{M}}(k_x, k_z)|^2$ in the central (annular) region was defined as a measure of ferromagnetic (crystalline) order.

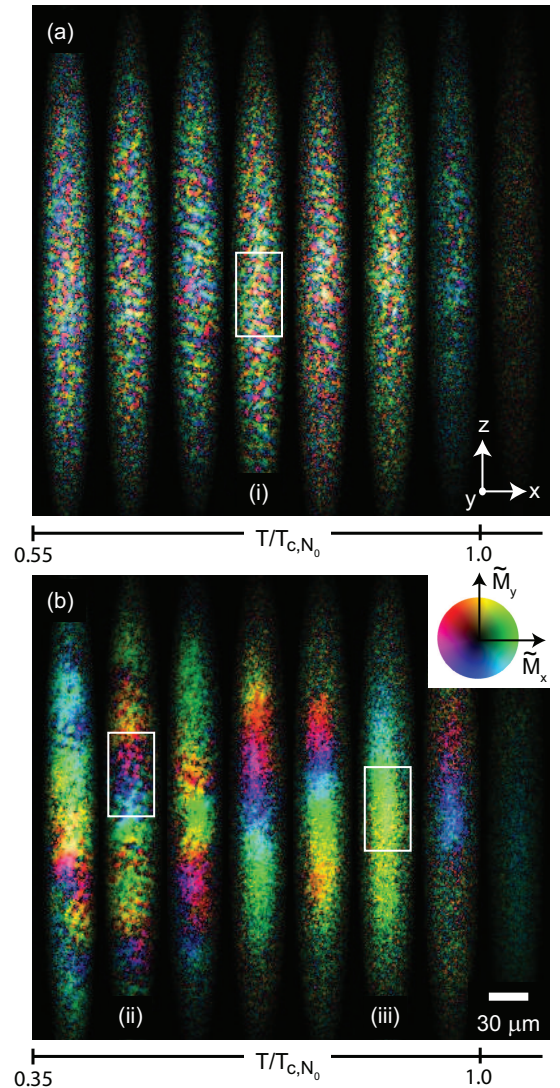


FIG. 1: Magnetic phases of ^{87}Rb $F = 1$ spinor gases produced by cooling thermal spin mixtures with initial values (a) $\eta = 0$ and (b) $\eta = 1/4$. The transverse magnetization $\tilde{M}_{x,y}$ (color wheel shown) of gases at various temperatures is shown as a function of position in the \hat{x} - \hat{z} plane. Temperatures are scaled by the Bose condensation temperature given the trap parameters and the population of the $|m_F = 0\rangle$ state. Portions of the textures labeled (i,ii,iii) are shown in detail in Fig. 2.

These measures distinguish between spin textures obtained from differing initial conditions (Fig. 3). For $\eta = 0$, the crystalline order becomes non-zero immediately below T_{c,N_0} and rises monotonically with decreasing temperature, remaining a constant fraction of the spectral power expected for a fully magnetized condensate. The ferromagnetic order remains small at all temperatures indicating that the average vector magnetization over length scales larger than $\sim 20 \mu\text{m}$ is roughly zero.

In contrast, for $\eta = 1/4$, ferromagnetic order dominates below T_{c,N_0} down to $0.75(3)T_{c,N_0} = 170(50)$ nK. Below this temperature, crystalline order emerges and

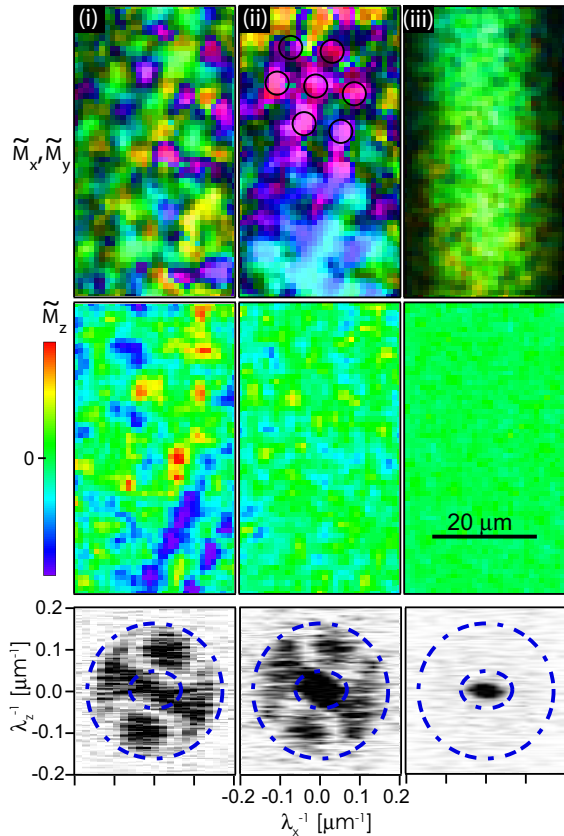


FIG. 2: Detailed examination of spin textures observed at conditions {initial η , final $T/T_{c,N_0}$ } given as {0, 0.68} (left), {1/4, 0.45} (middle), and {1/4, 0.85} (right), corresponding to regions (i), (ii), and (iii) of Fig. 1, respectively. The transverse (top, using color scheme of Fig. 1) and longitudinal (middle, color scale shown) magnetization, and also the vector magnetization spatial power spectrum (bottom, gray scale), are shown. Crystalline spatial order is observed directly in (i) and (ii), and also in Fourier space by the spectral features at $\lambda^{-1} \equiv k/2\pi \sim 0.1 \mu\text{m}^{-1}$. In contrast, the $\eta > 0$ high temperature phase is spatially uniform. Order parameters for the ferromagnetic (crystalline) phase are defined as the integrated power within the inner ellipse (annular region) shown in dashed lines.

coexists with ferromagnetism. We note that the above temperature corresponds roughly with the dipolar energy between neighboring domains of the spin lattice $\epsilon_d \sim \frac{\mu_0}{4\pi} \mu^2 \tilde{n}^2 l = k_B \times 210 \text{ nK}$. This correspondence suggests that the transition to the crystalline phase is mediated by the magnetic dipole interaction. We note also that the degenerate spinor gas is effectively two-dimensional, with its Thomas-Fermi radius along the direction of tightest confinement, $r_y \simeq 1.5 \mu\text{m}$, being smaller than the spin healing length $\xi = \hbar/(2m|c_2|n)^{1/2}$. In this context, it is conceivable that this transition marks the defect-induced melting of the quantum crystalline solid [20].

The phenomenological differences between the gases cooled from $\eta = 0$ and $\eta = 1/4$ may be explained in part by the different manners in which their magnetiza-

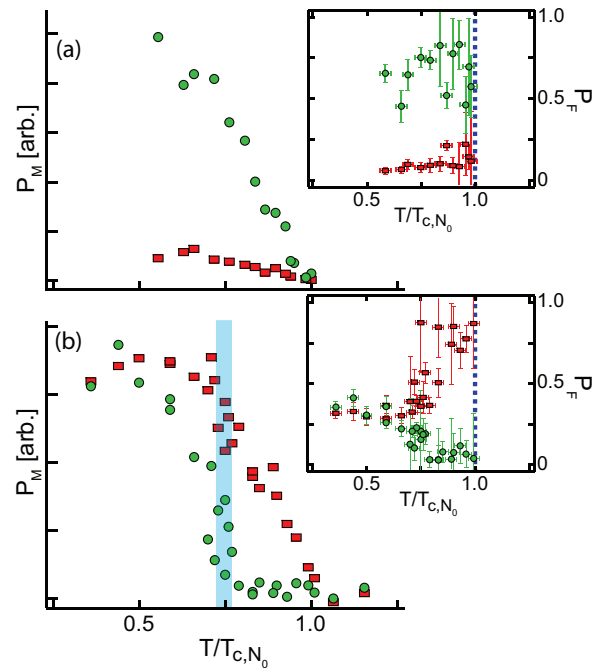


FIG. 3: Ferromagnetic (red rectangles) and crystalline (green circles) order parameters are defined as the sums $P_M = \sum_k |\mathbf{M}(k_x, k_y)|^2$ in regions of spatial Fourier space defined in Fig. 2. Insets show these order parameters as fractions of the integrated spectral power expected for a uniformly magnetized condensate. (a) Gases cooled from $\eta = 0$ show a single transition to a phase dominated by crystalline order. (b) Data for $\eta = 1/4$ show an additional transition between coexisting ferromagnetic and crystalline order at low temperature and solely ferromagnetic order at high temperature.

tion originates. For $\eta = 0$, magnetization may appear directly upon Bose-Einstein condensation, with the thermal cloud providing no preferential magnetization orientation. In contrast, for $\eta > 0$, Bose condensation occurs first in the dominant $|m_F = 0\rangle$ state. At low values of the quadratic Zeeman energy, $q < q_0 \simeq 2|c_2|n$, this unmagnetized condensate is subject to a spin-mixing instability [21], whereby it serves as a source for magnetization that lies preferentially in the transverse plane. This timeline was verified by experiments in which we probed gases at different times during their evaporation and equilibration. Indeed, with $\eta = 1/4$, unmagnetized condensates in the $|m_F = 0\rangle$ state were observed before the appearance of magnetization. Further, at $q = h \times 70 \text{ Hz} > q_0$, for which a $|m_F = 0\rangle$ condensate is stable, a similar cooling sequence resulted neither in a condensate fraction in the $|m_F = \pm 1\rangle$ states nor in the appearance of transverse magnetization.

One intriguing feature of the crystalline magnetic phase is the emergence of an axis in spin space along which the magnetization exhibits the largest variance. To identify this axis, we considered the distribution of vector spins measured at each imaged pixel within $30 \times 20 \mu\text{m}^2$ regions of the gas (Fig. 4). These re-

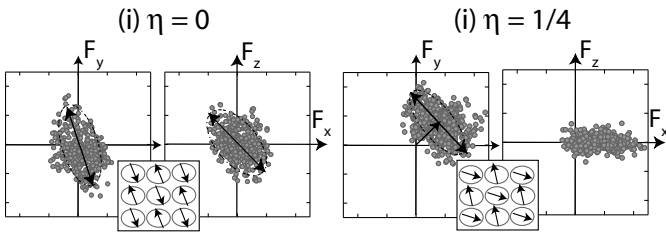


FIG. 4: Crystalline spin textures are characterized by a spin-space axis along which their magnetization is modulated. The spin distribution ($\langle \mathbf{F} \rangle$) within regions spanning $20 \mu\text{m}$ along \hat{z} and $30 \mu\text{m}$ along \hat{x} are shown; these regions are at the center of those shown in Figs. 1, 2. For $\eta = 0$ (i), both transverse (F_x, F_y) and longitudinal (F_z) spin modulations are evident, while for $\eta = 1/4$ (ii) the modulation is only transverse. The long axis of the prolate spin distribution defines the local spin axis (indicated by double-headed arrow). For $\eta = 1/4$, this distribution is offset from zero due to non-zero ferromagnetic order coexisting with the crystalline spin modulation. The dashed ellipses are guides to the eye.

gions were centered on the condensate in the \hat{x} direction while the location along the long axis (\hat{z}) was allowed to vary. The observed spin-space distribution was significantly prolate, and the long axis of this distribution was identified as the local spin axis [17]. This spin axis varies over characteristic distances of $\simeq 30 \mu\text{m}$ across the length of the spin texture, matching the extent of significant spatial magnetization correlations. For $\eta = 0$, the spin axis samples all of spin space, while it is confined to the transverse plane for $\eta > 0$.

The limited lifetime (about 1 s) of our gaseous samples restricted the duration over which they were allowed to equilibrate. This restriction raises the question of whether the observed magnetic phases represent long-lived metastable states, dynamical steady states or true equilibrium phases. To help address this question, we have verified that both the temperature and the popula-

tions of the non-condensate fractions reach equilibrium within 100 - 150 ms of the establishment of the final trap depth, well within the equilibration period. Doubling the evaporation time or lengthening the equilibration period to as long as 1 s produced no discernible changes in the magnetic order, other than overall loss in atom number. In addition to the studies presented here, we have also observed similar crystalline phases following the dissolution of helical spin textures [8] as well as after sufficiently long evolution times following a quantum quench of an unmagnetized condensate into a magnetic state [21]. Altogether, these studies suggest that the crystalline textures are either a low-temperature equilibrium configuration of this dipolar fluid, or at the very least, a robust metastable state.

In conclusion, we observe stable, self-organized crystalline spin textures in an ultracold dipolar spinor gas under a variety of initial conditions. An intriguing question arises regarding the superfluid properties of this dipolar quantum fluid. The observation of bimodal density distributions in time-of-flight images and the agreement between the fractional populations in this bimodal distribution and the expected Bose condensate fraction suggest the presence of a weakly interacting three-dimensional Bose condensate (and hence, a superfluid). A measurement of long-range phase coherence would conclusively establish the presence of a superfluid co-existing with the magnetic lattice, thereby supporting the existence of supersolidity in this dipolar magnetic fluid.

We thank T.L. Ho, J. Moore and A. Vishwanath for valuable discussions. This work was supported by the NSF, and by the DARPA OLE program (ARO Grant No. W911NF-07-1-0576). Partial personnel and equipment support was provided by the Division of Materials Sciences and Engineering, Office of Basic Energy Sciences. S.R.L. acknowledges support from NSERC and F.S. from the Gottlieb Daimler and Karl Benz Foundation.

-
- [1] E. Kim and M. H. W. Chan, *Nature* **427**, 225 (2004).
 - [2] J. Orenstein and A. J. Millis, *Science* **288**, 468 (2000).
 - [3] J. E. Hoffman et al., *Science* **295**, 466 (2002).
 - [4] G. C. Milward, M. J. Calderon, and P. B. Littlewood, *Nature* **433**, 607 (2005).
 - [5] S. Sachdev, *Science* **288**, 475 (2000).
 - [6] M. Seul and D. Andelman, *Science* **267**, 476 (1995).
 - [7] E. Dagotto, *Science* **309**, 257 (2005).
 - [8] M. Vengalattore, S. Leslie, J. Guzman, and D. Stamper-Kurn, *Phys. Rev. Lett.* **100**, 170403 (2008).
 - [9] H. Schmaljohann et al., *Phys. Rev. Lett.* **92**, 040402 (2004).
 - [10] M.-S. Chang et al., *Phys. Rev. Lett.* **92**, 140403 (2004).
 - [11] T.-L. Ho, *Phys. Rev. Lett.* **81**, 742 (1998).
 - [12] T. Ohmi and K. Machida, *J. Phys. Soc. Jpn.* **67**, 1822 (1998).
 - [13] S. Yi, L. You, and H. Pu, *Phys. Rev. Lett.* **93**, 040403 (2004).
 - [14] S. Yi and H. Pu, *Phys. Rev. Lett.* **97**, 020401 (2006).
 - [15] Y. Kawaguchi, H. Saito, and M. Ueda, *Phys. Rev. Lett.* **98**, 110406 (2007).
 - [16] J. Higbie et al., *Phys. Rev. Lett.* **95**, 050401 (2005).
 - [17] See EPAPS Document No. [XXX] for details on time-of-flight imaging data, the spatial correlations of the magnetization, and the identification of the local spin axis for the crystalline phase. For more information on EPAPS, see <http://www.aip.org/pubservs/epaps.html>.
 - [18] M. Vengalattore et al., *Phys. Rev. Lett.* **98**, 200801 (2007).
 - [19] R. Cherng and E. Demler, preprint arXiv:0806.1991 (2008).
 - [20] J. M. Kosterlitz and D. J. Thouless, *J. Phys. C* **6**, 1181 (1973).
 - [21] L. Sadler et al., *Nature* **443**, 312 (2006).